Mon. Not. R. Astron. Soc. **000**, 000–000 (1999)

Dust temperature and the submillimetre–radio flux density ratio as a redshift indicator for distant galaxies

A. W. Blain
Cavendish Laboratory, Madingley Road, Cambridge, CB3 0HE.

16 August 1999

ABSTRACT

It is difficult to identify the distant galaxies selected in existing submillimetre-wave surveys, because their positions are known at best to only several arcseconds. Centimetre-wave VLA observations are required in order to determine positions to subarcsecond accuracy, and so to allow reliable optical identifications to be made. Carilli & Yun pointed out that the ratio of the radio to submillimetre-wave flux densities provides a redshift indicator for dusty star-forming galaxies, when compared with the tight correlation between the far-infrared and radio flux densities observed in low-redshift galaxies. This method does provide a useful, albeit imprecise, indication of the distance to a submillimetre-selected galaxy. Unfortunately, it does not provide an unequivocal redshift estimate, as the degeneracy between the effects of increasing the redshift of a galaxy and decreasing its dust temperature is not broken.

Key words: galaxies: distances and redshifts – galaxies: general – galaxies: starburst – infrared: galaxies – radio continuum: galaxies

1 INTRODUCTION

The intensity of synchrotron radio emission from shock-heated electrons in star-forming galaxies is known to be correlated tightly with their far-infrared emission from dust grains heated by the interstellar radiation field (see the review by Condon 1992). This far-infrared–radio correlation arises because both radiation processes are connected with ongoing high-mass star formation activity in a galaxy. The correlation is described accurately by the equation,

$$S_{1.4\mathrm{GHz}} = [(1.7^{+1.0}_{-0.6}) \times 10^{-3}]\,(2.58 S_{60\mu\mathrm{m}} + S_{100\mu\mathrm{m}}), \qquad (1)$$

which links the flux densities of a galaxy in the 60- and 100-μm *IRAS* passbands and at a frequency of 1.4 GHz in the radio waveband, $S_{60\mu\mathrm{m}}$, $S_{100\mu\mathrm{m}}$ and $S_{1.4\mathrm{GHz}}$, respectively.

A reasonable pair of template spectral energy distributions (SEDs), which describe dusty galaxies at the relevant frequencies in equation (1), are shown in Fig. 1. The observed flux densities of the luminous dusty galaxy Arp 220 are also shown. The model SED derived in the far-infrared waveband by Blain et al. (1999b), based on *IRAS* and *ISO* galaxy counts, is continued into the radio waveband directly using equation (1). The SED and galaxy evolution models from that paper can be combined with the far-infrared–radio correlation (equation 1) to predict the counts of faint radio galaxies. The predicted count of galaxies brighter than 10 μJy at a wavelength of 8.4 GHz is 0.8 arcmin^{-2}, in excellent agreement with the observed value of 1.0 ± 0.1 arcmin^{-2} (Partridge et al. 1997).

The slope of the SED changes abruptly at a wavelength of about 3 mm, at which the dominant contribution to the SED changes from synchrotron radio emission to thermal dust radiation. Because the far-infrared–radio correlation links the flux densities on either side of this spectral break, it could be exploited to indicate the redshift of the galaxy (Carilli & Yun 1999). Carilli & Yun calculated that the radio–submillimetre flux density ratio of a distant dusty galaxy, which lies on the far-infrared–radio correlation, should be

$$\frac{S_{1.4\mathrm{GHz}}}{S_{850\mu\mathrm{m}}} = 3.763(1+z)^{1.007(\alpha_{\mathrm{radio}} - \alpha_{\mathrm{submm}})}, \qquad (2)$$

as a function of redshift z. α_{radio} and α_{submm} are the spectral indices of the SED, $S_\nu \propto \nu^\alpha$, in the radio and submillimetre wavebands, respectively. Typically, $\alpha_{\mathrm{radio}} \simeq -0.8$ and $\alpha_{\mathrm{submm}} \simeq 3.0$ to 3.5. The submillimetre-wave spectral index α_{submm} is the sum of the Rayleigh-Jeans spectral index ($\alpha = 2$) and β, the spectral index in the dust emissivity function $\epsilon_\nu \propto \nu^\beta$. Carilli & Yun also derived empirical flux density ratio–redshift relations from the SEDs of Arp 220 and M82. The spread of the redshift values that correspond to a fixed flux density ratio across their four models corresponds to an uncertainty in the predicted redshift of about ± 0.5.

The sensitive SCUBA submillimetre-wave camera at the JCMT (Holland et al. 1999) has been used to detect high-redshift dusty galaxies at a wavelength of 850 μm (see Barger, Cowie & Sanders 1999a and references within).

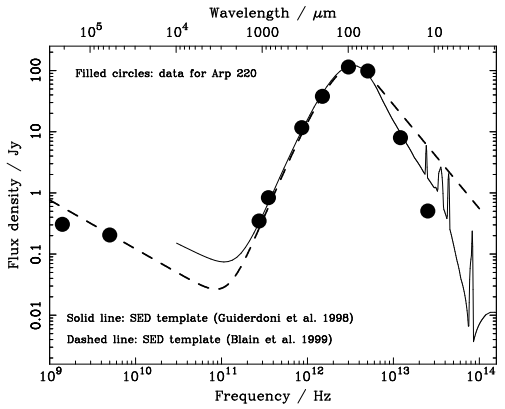

Figure 1. The template SEDs used to describe dusty galaxies by Guiderdoni et al. (1998; solid line) and Blain et al. (1999b; dashed line). The dashed line is normalized to match the far-infrared–radio correlation described in equation (1) (Condon 1992). At wavelengths longer than about 3 mm, the SED is dominated by synchrotron radio emission with a spectral index $\alpha_{\rm radio} \simeq -0.8$. At shorter wavelengths the SED is dominated by the thermal radiation from dust grains with an emissivity index $\beta = 1.5$ and a temperature $T = 38\,{\rm K}$. The observed SED of Arp 220 (filled circles) is also shown. Guiderdoni et al.'s template includes mid-infrared spectral features (see Xu et al. 1998).

These galaxies are probably the high-redshift counterparts to the low-redshift ultraluminous infrared galaxies, and so their SEDs might be expected to follow the far-infrared–radio correlation. In this case, the ratios of their radio and submillimetre-wave flux densities could be substituted into equation (2) to indicate their redshifts.

The observed radio and submillimetre-wave flux densities of the submillimetre-selected galaxies SMM J02399−0136 (at $z = 2.808 \pm 0.002$; Frayer et al. 1998; Ivison et al. 1998) and SMM J14011+0252 (at $z = 2.5653 \pm 0.0003$; Frayer et al. 1999; Ivison et al. submitted), the $z = 4.69$ QSO BR 1202−0725 (Isaak et al. 1994; Kawabe et al. 1999), the $z = 2.29$ galaxy *IRAS* F10214+4724 (Rowan-Robinson et al. 1993) and the $z = 0.02$ *IRAS* galaxy Arp 220 can be substituted into equation (2) to obtain predictions for their redshifts. If $\alpha_{\rm submm} = 3.0$, then these are $z = 2.9 \pm 0.3$, 3.8 ± 0.4, 3.9 ± 0.5, 2.8 ± 0.2 and 1.1 ± 0.1 respectively; if $\alpha_{\rm submm} = 3.5$, then $z = 2.3 \pm 0.3$, 3.3 ± 0.4, 3.1 ± 0.4, 2.2 ± 0.3 and 1.0 ± 0.1 respectively. The technique provides a coarse indication of the redshift of these five galaxies, which are all known to lie at redshifts within the bounds of the range of predictions made by Carilli & Yun's four models. For an application of this method to the radio and submillimetre-wave fluxes of galaxies detected in the SCUBA lens survey see Smail et al. (1999). What are the systematic effects that limit the reliability of the inferred redshifts?

2 THE FAR-INFRARED–RADIO CORRELATION AT HIGH REDSHIFTS

The far-infrared–radio correlation is based on observations of a range of low-redshift galaxies: low- and high-luminosity spiral galaxies, irregular star-forming dwarf galaxies and more luminous infrared galaxies, with luminosities up to about $5 \times 10^{11} h^{-2}\,{\rm L}_\odot$. One factor that could modify the general properties of the SEDs of dusty galaxies at high redshifts is the increase in the temperature of the cosmic microwave background radiation (CMBR) from its value $T_{\rm CMBR} = 2.726\,{\rm K}$ at $z = 0$, as $(1 + z)$. If a certain type of galaxy contains dust at a temperature T_0 at $z = 0$, then the dust temperature of an identical galaxy at redshift z would be approximately,

$$T(z) = \left\{ T_0^{4+\beta} + T_{\rm CMBR}^{4+\beta} \left[(1+z)^{4+\beta} - 1 \right] \right\}^{1/(4+\beta)}. \qquad (3)$$

The bolometric far-infrared luminosity of the galaxy is not changed, and so the SED in the radio waveband should remain the same.

The increasing temperature of the CMBR has one further effect. There is a redshift above which the energy density in the CMBR exceeds that in the magnetic field in the interstellar medium of the observed galaxy. Thus synchrotron radio emission will be suppressed due to the cooling of the relativistic electrons by the inverse Compton scattering of CMBR photons at all higher redshifts. Carilli & Yun (1999) estimate that this will typically occur at redshifts $z \gtrsim 6$ for ultraluminous infrared galaxies and at $z \gtrsim 3$ for a high-redshift analogue of the Milky Way (Carilli, private communication). This effect is not included in the calculations carried out below; however, the potential deficit in the radio flux density from ultraluminous galaxies at $z \gtrsim 6$ should be borne in mind.

The SED from a galaxy at any frequency in the radio, submillimetre and far-infrared wavebands can be found by adding the spectrum of thermal dust emission, $f_\nu(T)$, to the associated radio spectrum derived using equation (1). However, the relative normalization of the radio and far-infrared spectra depends on the dust temperature T (see Fig. 2). Because the far-infrared–radio correlation is defined at $z = 0$, the increasing CMBR temperature at higher redshifts, discussed above, affects the SED in the far-infrared waveband but not in the radio waveband. The full expression for the flux density of a galaxy at redshift z at an observing frequency ν is,

$$S_\nu \propto \left[(1.7^{+1.0}_{-0.6}) \times 10^{-3} \right] \left[2.58 f_{\rm 5THz}(T_0) + f_{\rm 3THz}(T_0) \right] \times \left[\frac{\nu(1+z)}{1.4\,{\rm GHz}} \right]^{\alpha_{\rm radio}} + f_{\nu(1+z)}[T(z)] \, \frac{\int f'_\nu(T_0)\,{\rm d}\nu'}{\int f'_\nu[T(z)]\,{\rm d}\nu'}. \qquad (4)$$

$f_{\rm 5THz}$ and $f_{\rm 3THz}$ are the flux densities obtained after integrating the SED f_ν across the 60- and 100-μm *IRAS* passbands and dividing by the bandwidth, respectively. Equation (4) can be used to predict the 1.4-GHz and 850-μm flux densities, which are required to investigate the reliability of the radio–submillimetre flux density ratio as a redshift indicator. The subtle modification introduced to the ratio by the greater CMBR temperature at high redshifts is included. This correction is expected to be most significant for either cool galaxies with $T_0 \lesssim 20\,{\rm K}$ or very high-redshift galaxies at $z \gtrsim 10$.

3 UNCERTAINTIES

Galaxies with a range of different dust temperatures have flux density ratios that lie on the far-infrared–radio corre-

lation. This is because the far-infrared flux densities in the correlation (equation 1) are evaluated at 60- and 100-μm, wavelengths close to the peak of the SED of a typical dusty galaxy. Hence, shifting the position of the peak of the SED, by changing the dust temperature T, makes little difference to the bolometric far-infrared flux density and thus to the far-infrared–radio flux density ratio. This weak temperature dependence is illustrated in Fig. 2, in which the constant of proportionality in the far-infrared–radio correlation (equation 1) is shown as a function of dust temperature T. The radio flux density is assumed to be proportional to the bolometric far-infrared luminosity, and the far-infrared SED is assumed to take the form shown in Fig. 1, with $\beta = 1.5$. The radio flux density is then divided by the far-infrared flux density in the 60- and 100-μm *IRAS* passbands to yield the constant of proportionality, which is assumed to match the standard value of 1.7×10^{-3} exactly if $T = 50\,\mathrm{K}$. The horizontal dotted lines in Fig. 2 show the magnitude of the observed scatter in the empirical far-infrared–radio correlation (Condon 1992). Hence, the dispersion in the relation expected owing to different dust temperatures throughout the wide range from 20 to 70 K is only comparable with the intrinsic scatter in the correlation.

However, the effect of modifying either the dust temperature T or the emissivity index β on the ratio of the flux densities of a star-forming galaxy in the submillimetre and radio wavebands is much greater, as shown by the five different model SEDs in Fig. 3. Three different dust temperatures $T = 20$, 40 and 60 K are included, each with an emissivity index $\beta = 1.5$. In addition, the SED is calculated for the $T = 40\,\mathrm{K}$ model with $\beta = 1.0$ and 2.0.

The predicted forms of the submillimetre–radio flux density ratio as a function of redshift for all five of the template SEDs shown in Fig. 3 are calculated using equation (4) and shown in Fig. 4(a). The results of Carilli & Yun (1999), calculated using equation (2), are also shown for comparison. Carilli & Yun's equation provides a good description of the 1.4-GHz:850-μm flux density ratio if the dust temperature at $z = 0$, $T_0 \gtrsim 60\,\mathrm{K}$. However, the positions of the curves in Fig. 4(a) can be quite different if the dust temperature $T_0 \lesssim 60\,\mathrm{K}$. Hence, the redshift that would be assigned to a galaxy using the 1.4-GHz:850-μm flux density ratio alone, in the absence of knowledge of both the appropriate dust temperature and emissivity index, is very uncertain. This is true even if the far-infrared–radio correlation is assumed to be free from any intrinsic scatter, and any additional contribution to the radio flux density from an active galactic nucleus (AGN) is neglected. The scatter in the far-infrared–radio correlation is about 0.2 dex, and because the power-law index of the lines in Fig. 4(a) is about -2 at $z \sim 2$, an additional 0.1 dex ($\simeq 25$ per cent) uncertainty would be expected. See Carilli & Yun (1999) for a discussion of the effects of AGN.

It is interesting to replot the curves in Fig. 4(a) as a function of the combined redshift–dust temperature parameter $(1 + z)/T$. This is the quantity that is constrained by measuring the position of the peak of the thermal dust emission component of the SED by combining observations in the far- and mid-infrared wavebands (Blain 1999a). The results are shown in Fig. 4(b). Because the radio flux density is produced by a non-thermal emission mechanism, a measurement of the submillimetre–radio flux density ratio might

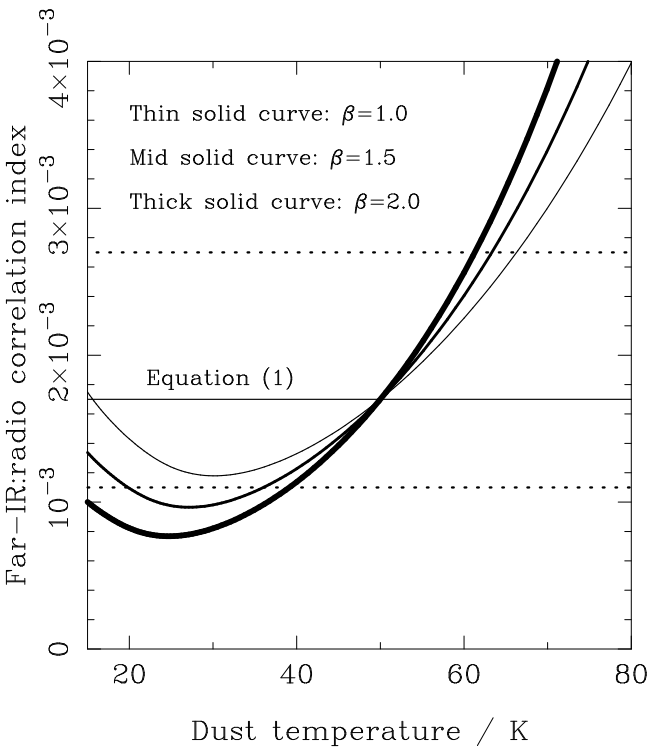

Figure 2. The constant of proportionality predicted in the far-infrared–radio correlation (equation 1) as a function of dust temperature. The radio flux density is assumed to be proportional to the bolometric far-infrared luminosity. The far-infrared flux density in the *IRAS* passbands (equation 1) is obtained by integrating the SED over these passbands and adding the results in the appropriate proportion. The observed value of the constant and its uncertainty are shown by the horizontal solid and dotted lines respectively. The predictions are normalised to the observed relation at a temperature of 50 K, which is typical of observed ultraluminous infrared galaxies.

be expected to break the degeneracy between temperature and redshift. However, because the differences between the curves in Fig. 4(b) are not much greater than the scatter in the far-infrared–radio correlation, the degeneracy remains.

3.1 Dust temperatures in luminous infrared galaxies

Uncertainties in the dust temperature of submillimetre-selected galaxies can lead to a significant uncertainty in the redshift that would be derived from the relations shown in Fig 4(a). What is known about the dust temperatures of galaxies and quasars?

In spiral galaxies, for example the Milky Way (Sodroski et al. 1997) and NGC 891 (Alton et al. 1998; Israel, van der Werf & Tilanus 1999), the observed SED can be adequately represented by a combination of different dust components with temperatures in the range from 15 to 30 K. In the core of NGC 891, Israel et al. (1999) report a compact component of warmer dust at $T \gtrsim 50\,\mathrm{K}$.

Franceschini, Andreani & Danese (1997) observed a sample of low-redshift 60-μm *IRAS* galaxies at a wavelength

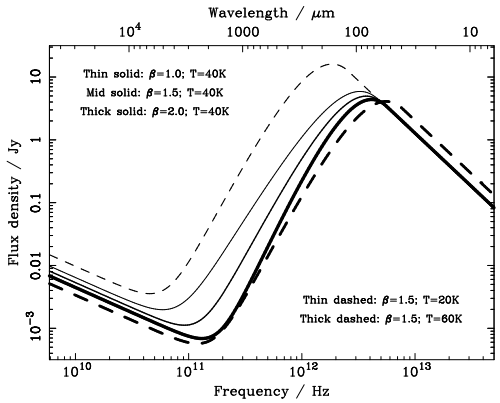

Figure 3. Examples of SEDs defined by different values of the $z = 0$ dust temperature T_0 and dust emissivity index β, all normalised to the same flux density at 60-μm. The SEDs are very different in the submillimetre waveband, but very similar at both far-infrared wavelengths of 60 and 100 μm and in the radio waveband. The 1.4-GHz:850-μm flux density ratios predicted in all five models shown here are compared in Fig. 4.

of 1.25 mm, the luminosities of which were distributed between 10^9 and 10^{11} $L_\odot$. The ratio of the 60-μm and 1.25-mm flux densities of these galaxies contains some information about the emissivity index and temperature of their interstellar dust. If only a single population of isothermal dust is present, then the scaling relation reported between the flux density ratio and the bolometric luminosity $L_{\rm bol}$ of the galaxies can be converted directly into a dust temperature–luminosity relation. If the emissivity index $\beta = 1.0$, then the dust temperature $T/{\rm K} \simeq 34(L_{\rm bol}/10^{10}\,{\rm L}_\odot)^{0.07}$, and if $\beta = 1.5$, then $T/{\rm K} \simeq 25(L_{\rm bol}/10^{10}\,{\rm L}_\odot)^{0.03}$. Hence, in this sample, dust temperatures appear to be relatively cool and there is only a weak dependence of temperature on luminosity. Note, however, that the 1.25-mm flux densities observed in this sample could be enhanced by the presence of either synchrotron/free–free radio emission or an energetically insignificant population of cool dust grains in the observed galaxies, as can be seen from the shape of the SEDs shown in Fig. 3. The dust temperature required to account for the data would be increased if any of these contributions were present. An extensive survey being carried out by Dunne et al. (1999) using SCUBA at shorter wavelengths of 450 and 850 μm will provide a more definitive result.

For more luminous galaxies, temperatures fitted to the observed SEDs of low-redshift ultraluminous infrared galaxies, such as Arp 220 and Mrk 231, tend to lie close to 50 ± 10 K. This temperature also provides a reasonable fit to the SED of the two submillimetre-selected galaxies with known redshifts, SMM J02399−0136 and SMM J14011+0252 (Ivison et al. 1998, 1999), and to the temperature of the coolest dust component of the high-redshift galaxies and quasars that were observed at a wavelength of 350-μm by Benford et al. (1999). For the three exotic gravitationally lensed high-redshift dusty galaxies and quasars selected in a variety of ways, IRAS F10214+4724, the Cloverleaf quasar H 1413+117 and APM 08279+5255, higher dust temperatures are typically found, in the range 75, 75 and 110 K respectively (see the discussion of their SEDs by Blain 1999b).

In order to provide consistent fits to the background radiation intensity and source counts in the far-infrared and submillimetre wavebands, assuming an isothermal population of high-redshift galaxies, both Blain et al. (1999b) and Trentham, Blain & Goldader (1999) found that typical dust temperatures of order 40 K were required. If a range of dust temperatures are considered, then 40 K is the likely luminosity-weighted average temperature.

The results of fits to the SEDs of dusty galaxies tend to indicate that dust temperatures are of order 20 K in low-luminosity spirals, of order 40–50 K in luminous *IRAS* galaxies, and perhaps higher in individual exotic high-redshift galaxies. At present, it seems reasonable to assume a temperature of order 40–50 K for submillimetre-selected galaxies in the absence of other information. If a temperature of 40 K is assumed, then the results of the Carilli & Yun (1999) formula (equation 2) are in reasonable agreement with the results of the calculations presented here at least if $\alpha_{\rm submm} = 3.5$ is assumed in equation (2).

A particular concern could be the potential misidentification of a submillimetre-selected galaxy with a low-redshift spiral galaxy, in which a dust temperature of about 20 K would be expected, rather than with a true, hotter and more distant counterpart, which would be expected to have the same value of $T/(1 + z)$. From Fig. 4(a), it is clear that a 20-K galaxy at $z \simeq 0.5$ and a 40-K galaxy at $z \simeq 2$ produce the same ratio of the 1.4-GHz and 850-μm flux densities. A real example of this type of degeneracy is seen in the combined submillimetre, radio, optical and near-infrared data that was used by Smail et al. (1999) to associate a background extremely red object (ERO) with a submillimetre source in the field of the cluster Cl 0939+47, rather than a $z = 0.33$ dusty spiral galaxy.

4 OTHER REDSHIFT INDICATORS

4.1 Mid- and far-infrared photometry

The 'redshifted dust temperature' of a galaxy, $T/(1 + z)$, can be determined by measuring the frequency of the peak of the far-infrared dust component of the SED (see Figs 1 and 3). Because of the thermal spectrum, the redshift z and the dust temperature T cannot be determined independently. Locating the peak frequency requires both long- and short-wavelength observations. These could be obtained by combining ground-based millimetre-wave observations, for example using the second-generation 1.1-mm bolometer camera BOLOCAM (Glenn et al. 1998), with far- and mid-infrared observations made at wavelengths of 24, 70 and 160 μm using the MIPS instrument on the *SIRTF* satellite: for more details see Blain (1999a).

4.2 Mid-infrared spectral features

Spectral features produced by emission from polycyclic aromatic hydrocarbons (PAHs) and atomic fine-structure lines in the restframe mid-infrared waveband at restframe wavelengths of order 10 μm (see Fig. 1) could be exploited to obtain photometric redshifts for distant galaxies (Xu et al. 1998). At shorter wavelengths, the prospects for obtaining

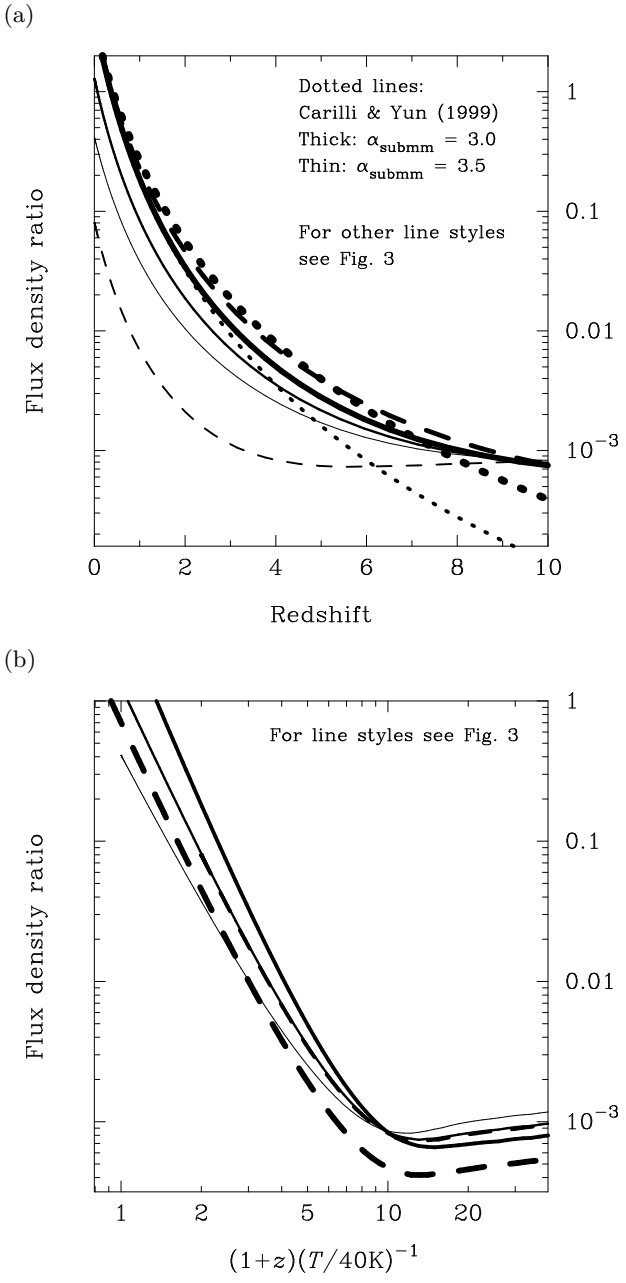

Figure 4. (a) The 1.4-GHz:850-μm flux density ratios expected for the five model SEDs shown in Fig. 3 as a function of redshift z. A considerable range of redshifts could be deduced from a measurement of this ratio if the temperature T or emissivity index β of the dust in the galaxy being observed was uncertain. The curves from Carilli & Yun (1999) are plotted assuming $\alpha_{\rm radio} = -0.8$. As stressed by Carilli & Yun, if the 1.4-GHz:850-μm flux density ratio is greater than 0.1, then the redshift z is likely to be less than 1, and if the ratio is less than 10^{-2}, then z is likely to be greater than 2. (b) The same flux density ratio plotted as a function of $(1 + z)/T$. In (b) the curves all overlap, indicating that it is difficult to break the degeneracy between the redshift z and dust temperature T of a galaxy using a measurement of the radio–submillimetre flux density ratio.

photometric redshifts using the 3–10-μm *SIRTF* IRAC camera have been discussed recently by Simpson & Eisenhardt (1999). Photometric redshifts deduced from these features will not be subject to the dust temperature–redshift degeneracy.

4.3 Submillimetre–optical flux density ratios

The identification of optical counterparts to submillimetre-selected galaxies usually requires a radio observation and a great deal of observing time (see for example Ivison et al. 1998, 1999). The optical magnitudes and colours of heavily-obscured submillimetre-luminous galaxies are expected to extend over wide ranges, and so the derivation of redshift information from broad-band optical photometry will probably require careful individual analysis of each submillimetre-selected galaxy. The results of photometric and spectroscopic observations of likely optical counterparts to submillimetre-selected galaxies (Smail et al. 1998; Barger et al. 1999b) are consistent with ratios of 850-μm and optical I-band flux densities that are scattered by about an order of magnitude across the sample.

5 PRACTICAL RADIO FOLLOW-UP OF FUTURE MILLIMETRE-WAVE SURVEYS

In order to exploit the redshift information provided by joint radio and submillimetre-wave observations, follow-up radio observations of submillimetre-selected galaxies must be acquired in a reasonable time.

In the next few years the most rapid survey for distant dusty galaxies will probably be made using the 1.1-mm BOLOCAM camera (Glenn et al. 1998). The detection rate of high-redshift galaxies at this wavelength is expected to be maximized at a survey depth of 10 mJy (Blain 1999a), based on the latest deep counts of galaxies detected by SCUBA (Blain et al. 1999a). At the Caltech Submillimeter Observatory (CSO), BOLOCAM should be able to map the sky to a 5σ sensitivity of 10 mJy at a rate of about $0.1\,{\rm deg}^2\,{\rm hr}^{-1}$, and detect galaxies at a rate of about $4\,{\rm hr}^{-1}$. Fitted to the US–Mexican 50-m Large Millimeter Telescope, the mapping speed would be $1.4\,{\rm deg}^2\,{\rm hr}^{-1}$ and the detection rate about $50\,{\rm hr}^{-1}$. For comparison, the mapping rate of SCUBA at 850 μm to the same flux density limit is about $10^{-5}\,{\rm deg}^2\,{\rm hr}^{-1}$, and the detection rate is about $0.2\,{\rm hr}^{-1}$ (Blain 1999a).

In order to detect the radio emission from the 90 per cent of BOLOCAM-selected galaxies that are expected to lie at $z \lesssim 5$ (Blain et al. 1999b), a 1.4-GHz VLA image that is about 300 times deeper in flux density than the BOLOCAM survey would be required. After the upgrade programme, the VLA will be able to reach the required 5σ sensitivity of 35 μJy in a 1-hr integration. The 30-arcmin primary beam of the VLA is expected to contain about 8 BOLOCAM detections. Hence, radio counterparts and thus temperature–redshift information can be obtained for the great majority of the galaxies detected in a millimetre-wave BOLOCAM/CSO survey, if about 15 per cent of the total time involved in the survey is spent at the upgraded VLA.

6 CONCLUSIONS

Radio observations of submillimetre-selected galaxies are crucial in order to make reliable optical identifications. The ratio of the radio and millimetre/submillimetre-wave flux densities also provides information about the redshift of the galaxy (Carilli & Yun 1999). However, the temperature and emissivity of dust in distant galaxies has a particularly significant effect on the ratio of the ratio of the submillimetre-wave and radio flux densities. For reasonable values of the dust emissivity and temperature, the radio–submillimetre flux density ratio cannot be used to break the degeneracy between the dust temperature and redshift of a distant dusty galaxy.

Acknowledgements

I thank Chris Carilli, Kate Isaak, Rob Ivison, Richard McMahon, Kate Quirk, Ian Smail, Min Yun and an anonymous referee for helpful comments. This research has made use of the NASA/IPAC Extragalactic Database (NED) which is operated by the Jet Propulsion Laboratory, California Institute of Technology, under contract with the National Aeronautics and Space Administration.

REFERENCES

Alton P. B., Bianchi S., Rand P. J., Xilouris E. M., Davies J. I., Trewhella M., 1998, ApJ, 507, L125
Barger A. J., Cowie L. L., Sanders D. B., 1999a, ApJ, 518, L5
Barger A. J., Cowie L. L., Smail I., Ivison R. J., Blain A. W., Kneib J.-P., 1999b, AJ, 117, 2656
Benford D. J., Cox P., Omont A., Phillips T. G., McMahon R. G., 1999, ApJ, 518, L65
Blain A. W., 1999a, in Weymann R., Storrie-Lombardi L., Sawicki M., Brunner R. eds, Photometric Redshifts, ASP conf. series, in press (astro-ph/9906141)
Blain A. W., 1999b, MNRAS, 304, 669
Blain A. W., Kneib J.-P., Ivison R. J., Smail I., 1999a, ApJ, 512, L87
Blain A. W., Smail I., Ivison R. J., Kneib J.-P., 1999b, MNRAS, 302, 632
Carilli C. L., 1999, private communication
Carilli C. L., Yun M. S., 1999, ApJ, 513, L13
Condon J. J., 1992, ARA&A, 30, 575
Dunne L. et al., 1999, MNRAS, submitted
Franceschini A., Andreani P., Danese L., 1998, MNRAS, 296, 709
Frayer D. T., Ivison R. J., Scoville N. Z., Yun M. S., Evans A. S., Smail I., Blain A. W., Kneib J.-P., 1998, ApJ, 506, L7
Frayer D. T. et al., 1999, ApJ, 514, L13
Glenn J. et al., 1998, in Phillips T. G. ed., Advanced Technology MMW, Radio and Terahertz telescopes. Proc. SPIE vol. 3357, SPIE, Bellingham, p. 326
Guiderdoni B., Hivon E., Bouchet F. R., Maffei B., 1998, MNRAS, 295, 877
Holland W. S. et al., 1999, MNRAS, 303, 659
Isaak K. G., McMahon R. G., Hills R. E., Withington S., 1994, MNRAS, 269, L28
Israel F. P., van der Werf P. P., Tilanus R. P. J., 1999, A&A, 344, L83
Ivison R. J., Smail I., Le Borgne J.-F., Blain A. W., Kneib J.-P., Bézecourt J., Kerr T. H., Davies J. K., 1998, MNRAS, 298, 583
Ivison R. J., Smail I., Barger A. J., Kneib J.-P., Blain A. W., Owen F. N., Kerr T. H., Cowie L. L., 1999, MNRAS, submitted
Kawabe R., Kohno K., Ohta K., Carilli C., 1999, in Carilli C. L., Radford S. J. E., Menten K., Langston G., Highly Redshifted Radio Lines. Astronomical Society of the Pacific, San Francisco, p. 45
Partridge R. B., Richards E. A., Fomalont E. B., Kellermann K. I., Windhorst R. A., 1997, ApJ, 483, 38
Rowan-Robinson M., et al., 1993, MNRAS, 261, 513
Simpson C., Eisenhardt P., 1999, PASP, 111, 691
Smail I., Ivison R. J., Blain A. W., Kneib J.-P., 1998, ApJ, 507, L21
Smail I., Ivison R. J., Owen F. N., Blain A. W., Kneib J.-P., 1999, ApJ, submitted (astro-ph/9907083)
Sodroski T. J., Odegard N., Arendt R. G., Dwek E., Weiland J. L., Hauser M. G., Kelsall T., 1997, ApJ, 480, 173
Trentham N., Blain A. W., Goldader J., 1999, MNRAS, 305, 61
Xu C. et al. 1998, ApJ, 508, 576